

DualFocus: Integrating Plausible Descriptions in Text-based Person Re-identification

Yuchuan Deng, Zhanpeng Hu, Jiakun Han, Chuang Deng, Qijun Zhao

School of Computer Science and Technology, Sichuan University, Chengdu, China
 {dengyuchuan, lucas, dengchuang}@stu.scu.edu.cn qjzhao@scu.edu.cn

Abstract

Text-based Person Re-identification (TPR) aims to retrieve specific individual images from datasets based on textual descriptions. Existing TPR methods primarily focus on recognizing explicit and positive characteristics, often overlooking the role of negative descriptions. This oversight can lead to false positives—images that meet positive criteria but should be excluded based on negative descriptions. To address these limitations, we introduce DualFocus, a unified framework that integrates plausible descriptions to enhance the interpretative accuracy of vision-language models in TPR tasks. DualFocus leverages Dual (Positive/Negative) Attribute Prompt Learning (DAPL), which incorporates Dual Image-Attribute Contrastive (DIAC) Learning and Sensitive Image-Attributes Matching (SIAM) Learning, enabling the detection of non-existent attributes and reducing false positives. To achieve a balance between coarse and fine-grained alignment of visual and textual embeddings, we propose the Dynamic Tokenwise Similarity (DTS) loss, which refines the representation of both matching and non-matching descriptions, thereby improving the matching process through detailed and adaptable similarity assessments. The comprehensive experiments on CUHK-PEDES, ICFG-PEDES, and RSTPReid, DualFocus demonstrates superior performance over state-of-the-art methods, significantly enhancing both precision and robustness in TPR.

Introduction

The rising demands for public safety and extensive surveillance networks have made manual tracking difficult, leading to the prominence of automatic person re-identification (Re-ID) (Ye et al. 2021). However, in cases where visual samples of an individual’s identity are unavailable, retrieval must rely solely on textual descriptions—a task known as Text-based Person Re-identification (TPR) (Li et al. 2017). Recent works in TPR (Yan et al. 2022; Zheng et al. 2020; Jiang and Ye 2023; Li et al. 2023b; Fujii and Tarashima 2023; Bai et al. 2023; Yang et al. 2023) have focused on enhancing the precision and efficiency of image retrieval and person recognition, leveraging Vision-Language Foundation Models (VLFM) such as CLIP (Radford et al. 2021) and ALIGN (Li et al. 2021). Traditionally, as illustrated in Figure 1, TPR methods have primarily concen-

trated on recognizing explicit, positively defined characteristics, such as ‘wearing a grey jacket.’ However, this focus often neglects negative descriptions—attributes identified as absent—such as ‘not wearing glasses.’ This oversight can result in false positives, where candidates that meet positive criteria are incorrectly retained because negative descriptions were not adequately considered. We posit that this inadequate management of negative descriptions in TPR may stem from the inherent difficulties VLFM faces in handling fine-grained tasks like attribute detection (Yao et al. 2021). To address this challenge, we introduce DualFocus, a



Figure 1: Illustration of the effect of negative descriptions. The green box signifies a triumphant retrieval, whereas the red box delineates a failed retrieval. Negative descriptions offer additional information that refines the search parameters, enabling a more accurate identification of an individual.

framework that highlights the importance of integrating both positive and negative descriptions. Central to this framework is the Dual Attribute Prompt Learning (DAPL) mechanism, which combines two key components: Dual Image-Attribute Contrastive (DIAC) Learning and Sensitive Image-Attributes Matching (SIAM) Learning. These components enhance the detection of unseen attributes while ensuring precise alignment between textual descriptions and image embeddings. Additionally, we propose the Dynamic Tokenwise Similarity (DTS) loss, a novel function that refines the alignment between textual narratives and visual representa-

tions. This approach meticulously aligns matching and mismatching descriptions at the token level, enabling dynamic similarity evaluation. Our results demonstrate that aligning fine-grained attributes within a unified embedding space and applying a balanced positive-negative granularity loss significantly improves the accuracy of complex attribute matching in DualFocus.

Our contributions can be summarized as follows:

- **Dual Attribute Prompt Learning (DAPL):** We introduce a novel approach that leverages both positive and negative descriptors to enhance the detection of previously unseen attributes. The integration of Dual Image-Attribute Contrastive (DIAC) Learning and Sensitive Image-Attributes Matching (SIAM) Learning enables precise alignment of textual descriptions with corresponding image patches, distinguishing our work from traditional attribute recognition methods.
- **DualFocus Framework:** Built on the DAPL mechanism, the DualFocus framework enhances CLIP’s ability to interpret complex textual descriptions through sophisticated fine-tuning. It carefully balances the integration of positive and negative descriptors, advancing the standard for text-based person retrieval.
- **Dynamic Tokenwise Similarity (DTS) Loss:** The DTS loss introduces a token-level similarity assessment. This dynamic evaluation mechanism fine-tunes the model’s sensitivity to attribute complexity and descriptive depth, significantly improving the alignment of attributes and the interpretation of subtle nuances across a diverse spectrum of textual queries.

Related work

Text-to-image Person Re-identification

The landscape of Text-based Person Re-identification (TPR) has evolved from a focus on global feature extraction (Chen et al. 2018; Han et al. 2021; Jiang and Ye 2023) to a more sophisticated emphasis on local feature alignment (Chen et al. 2022; Shao et al. 2022; Wang et al. 2022a; Yan et al. 2022). Although these methods enhance accuracy, they often introduce the trade-off of increased computational costs. Additionally, the integration of auxiliary tasks has emerged as a key strategy for implicit alignment, with studies (Jiang and Ye 2023; Shu et al. 2022; Ma et al. 2023; Bai et al. 2023) leveraging vision-language pretraining models to create superior representations, signaling a shift towards more integrated learning paradigms. An innovative approach by (Yang et al. 2023) introduces attribute prompt learning, utilizing attribute descriptions for precise image-attribute alignment while simultaneously enhancing text matching learning. Building on these developments, our strategy introduces dual attribute prompt learning, which uniquely integrates both positive and negative descriptions, moving beyond traditional methods focused solely on feature alignment or auxiliary tasks.

Vision-Language Pre-training

Recent advancements in Vision-Language Pretrained Models (VLP) have harnessed vast datasets of image-text pairs

to explore complex semantic interplays between visual and textual data. Central to these innovations is the “pre-training and fine-tuning” paradigm (Caron et al. 2021; Chen et al. 2020; He et al. 2020). Through this paradigm, models are meticulously refined across a spectrum of tasks, including image-text contrastive learning (Li et al. 2021; Radford et al. 2021; Yu et al. 2022), masked language modeling (Li et al. 2023a; Yu et al. 2022; Yao et al. 2021), and image caption generation (Dai et al. 2023; Li et al. 2023a). The result is the generation of contextually nuanced and semantically rich representations. These refined representations foster a deeper integration of visual and textual elements, markedly enhancing the efficacy of VLP models in downstream tasks.

Method

DualFocus Architecture

The Architecture Overview Figure 2 presents an overview of our DualFocus framework. The framework comprises six encoders: one Image Encoder (E_I), three Text Encoders (E_T) with shared weights, and two Cross Encoders (E_C) (Jiang and Ye 2023). The training dataset, denoted as $D = \{\mathbf{I}_i, \mathbf{T}_i\}_{i=1}^N$, consists of N image-text pairs, where each \mathbf{I}_i is an image of a person and \mathbf{T}_i is its corresponding textual description.

Generating Negative Descriptions The generation of negative descriptions, a critical component of our framework, involves identifying attributes from the predefined set \mathcal{A} that are explicitly absent in the textual description \mathbf{T}_i . This process begins with the comprehensive attribute set, which includes 27 predefined attributes commonly found in person descriptions, such as “wearing a hat,” “carrying a backpack,” or “having sunglasses.” For each textual description \mathbf{T}_i , we first identify the attributes that are explicitly mentioned, forming the set of positive attributes \mathbf{A}_i^p . The remaining attributes from the predefined set \mathcal{A} , which are not mentioned in \mathbf{T}_i , are classified as negative attributes \mathbf{A}_i^n . For instance, if the description states “a person wearing a red shirt and blue jeans,” attributes like “no hat,” “no sunglasses,” and “no backpack” would be generated as negative descriptions, assuming these attributes are part of the predefined set but are absent from the description. For each negative description, we select two absent attributes to generate it. For a given image, we create three distinct negative descriptions, ensuring that the selected attributes do not overlap across these descriptions.

Visual Representation Extraction. Given an input image \mathbf{I}_i , we initially divide it into a series of equally-sized, non-overlapping patches. These patches are then fed into an image encoder E_I , producing a set of high-dimensional embeddings $\{\mathbf{v}_k^i\}_{k=1,2,\dots,n_v}$. To capture the global features of the entire image, a learnable \mathbf{v}_{cls}^i token is incorporated. Consequently, the final visual representations are formulated as $\mathbf{F}_I^i = \{\mathbf{v}_{cls}^i, \mathbf{v}_1^i, \mathbf{v}_2^i, \dots, \mathbf{v}_{n_v}^i\}$.

Textual Representation Extraction. For the input text \mathbf{T}_i , we employ a Text Encoder E_T to map the textual information into a corresponding high-dimensional embedding space. Specifically, we process the text through

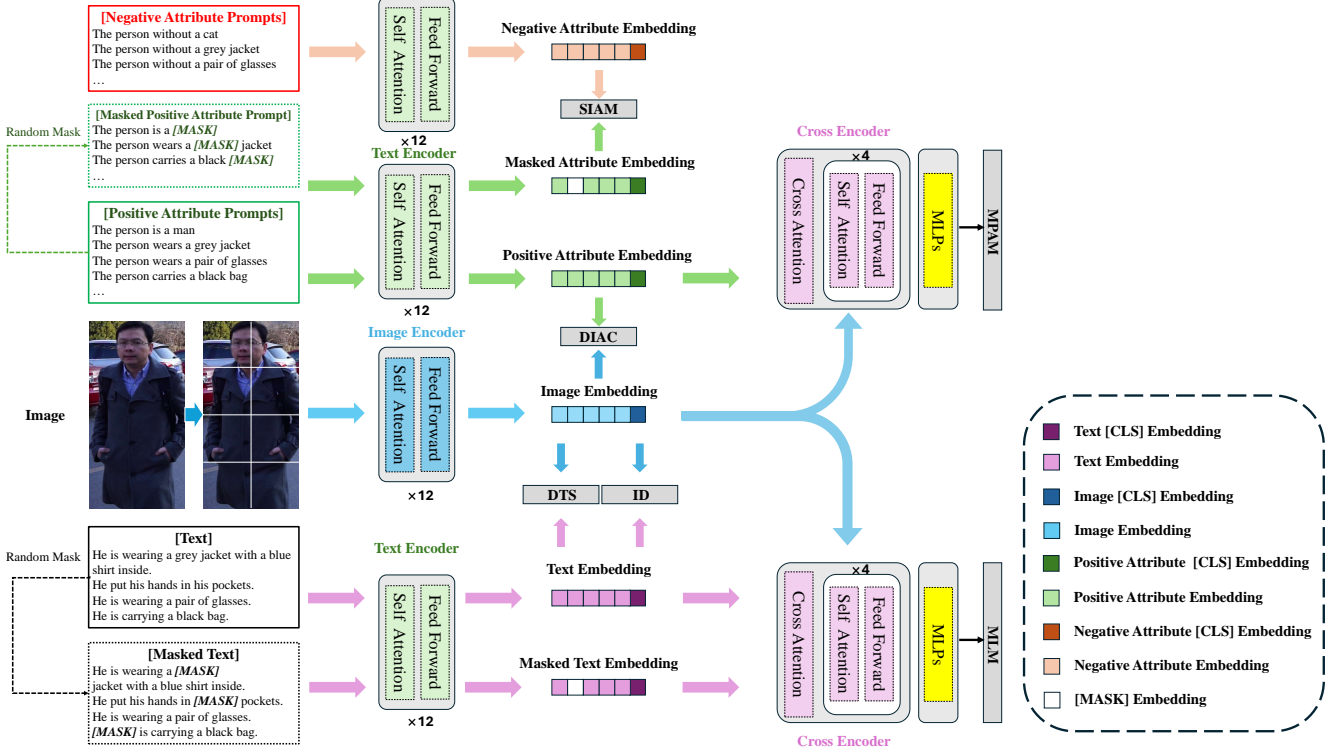


Figure 2: Overview of the proposed DualFocus framework. It consists of six encoders: one Image Encoder (E_I), three Text Encoders (E_T), and two Cross Encoders (E_C). The Image Encoder generates embeddings from visual inputs, while the Text Encoders produce embeddings from textual data. The Cross Encoders integrate these embeddings to enhance cross-modal prediction tasks. Text in grey boxes indicates tasks related to learning processes. Training strategies include Dual Image-Attribute Contrastive Learning (DIAC), which distinguishes images based on attributes; Sensitive Image-Attributes Matching Learning (SIAM), aligning attributes in text with images; Dynamic Tokenwise Similarity Loss (DTS), adjusting token similarity measures for accuracy; Masked Positive Attribute Language Modeling (MPAM), predicting masked positive attributes in context; and Masked Language Modeling (MLM), improving understanding by predicting missing words in sentences. Identity loss (ID), which ensures the preservation and recognition of individual characteristics across different modalities.

lower-case byte pair encoding (BPE) (Sennrich, Haddow, and Birch 2015) with a vocabulary size of 49,152. The resultant sequence of textual tokens is augmented with $[SOS]$ and $[EOS]$ tokens to denote the beginning and end of the sequence, respectively. Consequently, the final textual representations are formulated as $\mathbf{F}_T^i = \{\mathbf{t}_{sos}^i, \mathbf{t}_1^i, \mathbf{t}_2^i, \dots, \mathbf{t}_{n_t}^i, \mathbf{t}_{eos}^i\}$. Similarly, attribute descriptions are embedded as $\mathbf{F}_{A^p}^i$ for positive descriptions and $\mathbf{F}_{A^n}^i$ for negative descriptions.

Dynamic Tokenwise Similarity Loss

CLIP’s (Radford et al. 2021) reliance on global representations limits attribute precision within images. To address this, we combine token-level similarity computations (Yao et al. 2021) with SDM (Jiang and Ye 2023) loss to form the Dynamic Tokenwise Similarity (DTS) loss, enhancing fine-grained correspondences between image and text.

Given a batch of image features and text features $\{(\mathbf{F}_I^i, \mathbf{F}_T^j), y_{i,j}\}_{j=1}^B$, where B is the batch size and $y_{i,j}$ is a binary label indicating whether the pair $(\mathbf{F}_I^i, \mathbf{F}_T^j)$ shares

the same identity ($y_{i,j} = 1$ for a match, and $y_{i,j} = 0$ otherwise). For each visual token in \mathbf{F}_I^i , we compute its similarity with all tokens in \mathbf{F}_T^j , selecting the highest as the tokenwise maximum similarity $\xi_{i,j}^I$, for each image-text pair as follows:

$$\xi_{i,j}^I(\mathbf{F}_I^i, \mathbf{F}_T^j) = \frac{1}{n_v^i} \sum_{k=1}^{n_v^i} \text{sim}(\mathbf{v}_k^i, \mathbf{t}_{m_k^I}^j) \quad (1)$$

where $\text{sim}(\cdot)$ denotes the cosine similarity function. The index m_k^I , which corresponds to the maximal similarity for each visual token, is determined by:

$$m_k^I = \arg \max_{0 \leq r < n_t^j} \text{sim}(\mathbf{v}_k^i, \mathbf{t}_r^j). \quad (2)$$

This token-level comparison allows for capturing and contrasting features with greater detail. Non-padded tokens from image and text samples are represented as \mathbf{F}_I^i and \mathbf{F}_T^j , respectively. The probability of image-to-text matching $p_{i,j}^{2t}$

is evaluated using a softmax function, defined as:

$$p_{i,j}^{i2t}(\mathbf{F}_I^i, \mathbf{F}_T^j) = \frac{\exp(\xi_{i,j}^I(\mathbf{F}_I^i, \mathbf{F}_T^j)/\tau)}{\sum_{k=1}^B \exp(\xi_{i,k}^I(\mathbf{F}_I^i, \mathbf{F}_T^k)/\tau)}, \quad (3)$$

where τ is a temperature hyperparameter which controls the probability distribution peaks. Then the DTS loss from images to text in a mini-batch is computed by:

$$\mathcal{L}_{i2t} = \frac{1}{B} \sum_{i=1}^B \sum_{j=1}^B p_{i,j}^{i2t} \log \left(\frac{p_{i,j}^{i2t}}{q_{i,j}^{i2t} + \epsilon} \right), \quad (4)$$

where ϵ is a small constant added to prevent numerical instability. And $q_{i,j}^{i2t} = y_{i,j} / \sum_{k=1}^B y_{i,k}$ represents the true matching probability. Symmetrically, the DTS loss from text to image, \mathcal{L}_{t2i} , mirrors this by exchanging the roles of image and text. And the bi-directional DTS loss is denoted as:

$$\mathcal{L}_{dts} = \mathcal{L}_{i2t} + \mathcal{L}_{t2i}. \quad (5)$$

Dual Attribute Prompt Learning (DAPL)

Motivation To enhance the precision of attribute detection, we propose the Dual Attribute Prompt Learning (DAPL) approach. Diverging from the APL (Yang et al. 2023), DAPL distinctively leverages both positive and negative attribute descriptions. This innovation is primarily achieved through the integration of Dual Image-Attribute Contrastive Learning and Sensitive Attributes Prompt Matching Learning, significantly bolstering the detection of a wide array of attributes.

Dual Image-Attribute Contrastive Learning Dual Image-Attribute Contrastive (DIAC) Learning employs both positive and negative descriptions for contrastive learning at the token-level. Specifically, for each image \mathbf{I}_i within an image-attribute batch, we compute similarity scores for both types of descriptions against \mathbf{F}_I^i , as described in Eq. 4. For instance, the similarity score for a positive prompt is calculated using the following methodology:

$$S_p^{i2a} = p_{i,j}^{i2t}(\mathbf{F}_I^i, \mathbf{F}_{A_p}^i). \quad (6)$$

Similarly, similarity scores S_p^{a2i} , S_n^{i2a} and S_n^{a2i} are computed. Following (Yang et al. 2023), for positive attribute descriptions, the Positive Image-Attribute Contrastive Learning (PIAC) Loss is given by:

$$\mathcal{L}_{piac} = -\frac{1}{2B} \sum_{A_p^i \in \mathcal{A}} (\log S_p^{i2a} + \log S_p^{a2i}). \quad (7)$$

In a parallel manner, the Negative Image-Attribute Contrastive Learning (NIAC) Loss, \mathcal{L}_{niac} , is calculated, leading to the formulation of the Dual Image-Attribute Contrastive Learning (DIAC) Loss as:

$$\mathcal{L}_{diac} = \frac{1}{2} (\mathcal{L}_{piac} - \mathcal{L}_{niac}). \quad (8)$$

Sensitive Image-Attributes Matching Learning Sensitive Image-Attributes Matching Learning (SIAM) is designed to enhance the model's ability to accurately distinguish between positive and negative attribute descriptions, thereby improving the sensitivity to subtle differences in attribute presence or absence. In traditional approaches, the similarity scores between image features and attribute descriptions are crucial in determining the attribute probabilities $\mathbf{p}_{i,j}^a$. However, without careful balancing, models can become biased toward more frequently occurring attributes, potentially leading to inaccuracies in cases where attributes are either explicitly present or absent. To address this, we introduce a dynamic adjustment factor $\gamma_a^i = \frac{\text{Count}(A_p^i)}{\text{Count}(A_n^i)}$, which is designed to balance the sensitivity across attributes by adjusting the weighting between positive and negative examples for each attribute \mathbf{A}_i . This factor ensures that the model fairly evaluates both the presence and absence of attributes, preventing any one type from disproportionately influencing the attribute probabilities. The attribute probabilities $\mathbf{p}_{i,j}^a$ are computed using the following equation, where we sum over both positive ('p') and negative ('n') attributes:

$$\mathbf{p}_{i,j}^a = \frac{1}{2} \sum_{k \in \{p,n\}} \text{softmax} \left(\gamma_a^i S_k^{i2a} - \frac{1}{\gamma_a^i} S_k^{a2i} \right). \quad (9)$$

To further improve the matching of sensitive attributes, we employ a cross-entropy loss function:

$$\mathcal{L}_{siam} = -\frac{1}{B} \sum_{\mathbf{A}_i \in \mathcal{A}} \sum_{j=1}^B (y_{i,j} \log(\mathbf{p}_{i,j}^a) + (1 - y_{i,j}) \log(1 - \mathbf{p}_{i,j}^a)). \quad (10)$$

Masked Positive Attribute Language Modeling Masked Attribute Language Modeling (MAM) (Yang et al. 2023) is designed to predict masked words utilizing clues from matched pairs of images and attribute descriptions. Our implementation incorporates the Implicit Relation Reasoning Loss function (Jiang and Ye 2023) to refine the prediction of masked attributes. Specifically, we only focus on using masked positive attribute descriptions, and the loss function is represented as \mathcal{L}_{mapm} .

To calculate the overall performance of the Dual Attribute Prediction and Learning (DAPL) model, we integrate the contributions from various individual loss functions in a balanced manner:

$$\mathcal{L}_{dapl} = \frac{1}{3} (\mathcal{L}_{diac} + \mathcal{L}_{siam} + \mathcal{L}_{mapm}). \quad (11)$$

Overall Loss Function

The overall loss function for training our proposed method is defined as:

$$\mathcal{L} = \lambda_{dts} \mathcal{L}_{dts} + \lambda_{mlm} \mathcal{L}_{mlm} + \lambda_{id} \mathcal{L}_{id} + \lambda_{dapl} \mathcal{L}_{DAPL}, \quad (12)$$

where \mathcal{L}_{id} represents the Identity Loss (Zheng et al. 2020), and \mathcal{L}_{mlm} denotes the Implicit Relation Reasoning Loss (Jiang and Ye 2023) that utilizes masked text as input. The coefficients λ_{dts} , λ_{mlm} , λ_{id} , and λ_{dapl} are hyperparameters designed to balance the contributions of each component loss to the overall loss function.

Experiments

Experimental Setup

Datasets and Evaluation Metrics We evaluate our method on three text-based person Re-identification datasets: CUHK-PEDES (Li et al. 2017), ICFG-PEDES (Ding et al. 2021), and RSTPReid (Zhu et al. 2021). The effectiveness of the TPR system is assessed using multiple metrics. The primary metric is Rank- k , which measures the likelihood of a correct match appearing in the top- k results of a text query. In addition, we employ mean average precision (mAP) and mean Inverse Negative Penalty (Ye et al. 2021) (mINP) to provide a more comprehensive evaluation. mAP quantifies the precision of relevant image retrievals, while mINP reflects the average inverse penalties for relevant pairs, with higher scores across these metrics indicating superior performance.

Implementation Details We adopt the CLIP-ViT-B/16 model as our pre-trained image encoder and the CLIP text transformer as our text encoder (Radford et al. 2021). Additionally, we integrate a cross encoder as proposed by (Jiang and Ye 2023). Following (Jiang and Ye 2023; Li et al. 2023b), we input images are initially resized to 384×128 pixels and undergo a series of augmentations, including random horizontal flipping, random cropping with padding, random erasing, and normalization to enhance the robustness of the model. The maximum token sequence length, n_t , is configured to 77. For optimization, the Adam algorithm (Kingma and Ba 2015) is employed over 50 epochs, starting with a learning rate of 1×10^{-5} , and incorporating cosine decay to adjust the learning rate over time. The first 5 epochs serve as a warm-up period, during which the learning rate linearly increases from 1×10^{-6} to 1×10^{-5} . For modules initialized without pre-trained weights, the learning rate is set at 5×10^{-5} from the outset. In our (DTS) loss calculation, we set the temperature parameter τ to 0.02. The regularization parameters λ_{dts} and λ_{dapl} parameters adjusted to 2 and 0.8, respectively. The parameters λ_{mlm} and λ_{id} are both configured with a value of 1. Our models are implemented using PyTorch (Imambi, Prakash, and Kanagachidambaresan 2021) and trained on 4 NVIDIA RTX 4090 24G GPUs.

Comparison with State-of-the-Arts

Performance Comparisons on CUHK-PEDES As illustrated in Table 1, our DualFocus method outperforms a range of state-of-the-art (SOTA) techniques, particularly in Rank-1 accuracy where it achieves 77.43%, and mean Average Precision (mAP) at 68.35%. This is largely attributed to its local matching capability. Notably, unlike APTM (Yang et al. 2023), DualFocus was not pre-trained on the text-to-person synthetic dataset MALS, emphasizing its inherent efficiency. Beyond achieving high Rank-1 accuracy, DualFocus excels across a spectrum of metrics, marked by a remarkable mean Inverse Negative Penalty (mINP) of 53.56. This extensive performance is a testament to DualFocus’s prowess in person description retrieval.

Performance Comparisons on ICFG-PEDES As shown in Table 2, despite strong performance across several datasets, DualFocus achieves Rank-1 accuracy of 67.87% on the ICFG-PEDES dataset. This figure is slightly below the leading APTM (Yang et al. 2023) method, which records a Rank-1 accuracy of 68.51%, prompting a deeper analysis of the dataset’s unique challenges. However, DualFocus still performs well in Rank-5 and Rank-10 accuracy metrics and achieves a significant mINP of 9.14%, demonstrating its robustness in retrieving relevant queries from a large pool. A key feature of the ICFG-PEDES dataset is its privacy-preserving anonymization of faces, which removes crucial semantic details vital for accurate person identification. This reduction significantly affects DualFocus’s performance, underscoring the importance of facial and accessory cues in retrieval tasks. The impact of this anonymization reveals the limitations of current models, including DualFocus, in handling datasets where key identifying features are obscured, highlighting areas for future improvement in model adaptability.

Performance Comparisons on RSTPReid Results in Table 3 highlight DualFocus’s effectiveness on the RSTPReid dataset, achieving a Rank-1 accuracy of 69.12%, outperforming the APTM method. It also excels in Rank-5 and Rank-10 accuracies at 86.68% and 92.31%, respectively, and records a competitive mAP of 52.55% along with the highest mINP of 27.87%, confirming its consistent retrieval quality. This performance demonstrates DualFocus’s ability to handle the complexities of the RSTPReid dataset, utilizing CLIP-based visual-textual integrations to effectively recognize and differentiate individuals against variable backgrounds and orientations.

Overall, DualFocus consistently delivers excellent results across all benchmark datasets, proving the robustness and generalizability of our method.

Ablation Study

Effectiveness of the Dynamic Tokenwise Similarity (DTS) Loss Incorporating the Dynamic Tokenwise Similarity (DTS) loss function into the baseline model, identified as IRRA, results in significant improvements in Rank-1 accuracy across all datasets. The model’s performance increases to 74.09% on CUHK-PEDES, 65.24% on ICFG-PEDES, and 65.73% on RSTPReid. This improvement underscores the DTS loss’s capability in dynamically selecting challenging samples, thereby enhancing the model’s discriminative power and fine-grained matching precision over the Static Discriminative Margin (SDM) loss (Jiang and Ye 2023).

Effectiveness of Dual Attribute Prompts Learning (DAPL) The DAPL component, which synergistically combines \mathcal{L}_{diac} and \mathcal{L}_{siam} , further elevates the model’s performance. \mathcal{L}_{diac} maintains consistency across different representations of similar entities, whereas \mathcal{L}_{siam} focuses on refining the model’s sensitivity to variable data interactions, thereby reducing intra-class variations. Independently, each contributes significantly; however, their integration under

Table 1: Performance (%) comparisons with SOTA methods on CUHK-PEDES. Results are ordered based on the Rank-1 accuracy. In the "Type" column, "G" and "L" represent global matching and local matching methods, respectively. "-" indicates that the original paper did not use that specific metric to evaluate its models.

Method	Type	Image Enc.	Text Enc.	Rank-1	Rank-5	Rank-10	mAP	mINP
DSSL (Zhu et al. 2021)	L	RN50	BERT	59.98	80.41	87.56	-	-
SSAN (Ding et al. 2021)	L	RN50	LSTM	61.37	80.15	86.73	-	-
LBUL (Wang et al. 2022b)	L	RN50	BERT	64.04	82.66	87.22	-	-
Han et al. (Han et al. 2021)	G	CLIP-RN101	CLIP-Xformer	64.08	81.73	88.19	60.08	-
CAIBC (Wang et al. 2022a)	L	RN50	BERT	64.43	82.87	88.37	-	-
AXM-Net (Farooq et al. 2022)	L	RN50	BERT	64.44	80.52	86.77	58.73	-
IVT (Shu et al. 2022)	G	ViT-Base	BERT	65.59	83.11	89.21	-	-
BEAT (Ma et al. 2023)	L	RN101	BERT	65.61	83.45	89.57	-	-
CFine (Yan et al. 2022)	L	CLIP-ViT	BERT	69.57	85.93	91.15	-	-
IRRA (Jiang and Ye 2023)	G	CLIP-ViT	CLIP-Xformer	73.38	89.93	93.71	66.13	50.24
BiLMa (Fujii and Tarashima 2023)	G	CLIP-ViT	CLIP-Xformer	74.03	89.59	93.62	66.57	-
DECL (Li et al. 2023b)	G	CLIP-ViT	CLIP-Xformer	75.02	90.89	94.52	-	-
RaSa (Bai et al. 2023)	G	ALBEF-ViT	ALBEF-BERT	76.51	90.29	94.25	69.38	-
APTM (Yang et al. 2023)	L	ALBEF-ViT	ALBEF-BERT	76.53	90.04	94.15	66.91	-
DualFocus (Ours)	L	CLIP-ViT	CLIP-Xformer	77.43	90.73	94.20	68.35	53.56

Table 2: Performance (%) comparisons with SOTA methods on ICFG-PEDES dataset.

Method	Rank-1	Rank-5	Rank-10	mAP	mINP
Dual Path (Zheng et al. 2020)	38.99	59.44	68.41	-	-
ViTAA (Wang et al. 2020)	50.98	68.79	75.78	-	-
SSAN (Ding et al. 2021)	54.23	72.63	79.53	-	-
IVT (Shu et al. 2022)	56.04	73.60	80.22	-	-
BEAT (Ma et al. 2023)	58.52	75.92	81.96	-	-
CFine (Yan et al. 2022)	60.83	76.55	82.42	-	-
IRRA (Jiang and Ye 2023)	63.46	80.25	85.82	38.06	7.93
BEAT (Ma et al. 2023)	58.25	75.92	81.96	-	-
DECL (Li et al. 2023b)	64.88	81.34	86.72	-	-
RaSa (Bai et al. 2023)	65.28	80.40	85.12	41.29	-
APTM (Yang et al. 2023)	68.51	82.09	87.56	41.22	-
DualFocus (Ours)	67.87	81.93	87.13	40.13	9.14

Table 3: Performance (%) comparisons with SOTA methods on RSTPReid dataset.

Method	Rank-1	Rank-5	Rank-10	mAP	mINP
DSSL (Zhu et al. 2021)	39.05	62.60	73.95	-	-
SSAN (Ding et al. 2021)	43.50	67.80	77.15	-	-
LBUL (Wang et al. 2022b)	45.55	68.20	77.85	-	-
IVT (Shu et al. 2022)	46.70	70.00	78.80	-	-
CFine (Yan et al. 2022)	50.55	72.50	81.60	-	-
IRRA (Jiang and Ye 2023)	60.20	81.30	88.20	47.17	25.28
DECL (Li et al. 2023b)	61.35	83.95	90.45	-	-
BEAT (Ma et al. 2023)	48.10	73.10	81.30	-	-
RaSa (Bai et al. 2023)	66.90	86.50	91.35	52.31	-
APTM (Yang et al. 2023)	67.50	85.70	91.45	52.56	-
DualFocus (Ours)	69.12	86.68	92.31	52.55	27.87

DAPL leads to enhanced model performance with Rank-1 accuracies rising to 75.20% on CUHK-PEDES, 66.76% on ICFG-PEDES, and 67.07% on RSTPReid. These results highlight DAPL's crucial role in balancing input data aspects during training and refining the model's focus, thereby improving its understanding of complex visual-textual relationships.

Combined Effectiveness of DTS and DAPL The integration of both DTS and DAPL within the DualFocus configuration achieves the highest performance metrics across all evaluated datasets, indicating the synergistic effect of these components. This potent combination attains Rank-1 accuracies of 77.43% on CUHK-PEDES, 67.87% on ICFG-PEDES, and 69.12% on RSTPReid. The combined implementation not only reinforces the model's discriminative power but also significantly enhances its ability to accurately match textual descriptions with corresponding images, thereby setting a new benchmark in person description retrieval tasks.

Analysis of Sensitivity to Negative Descriptions

In this section, we evaluated the robustness of our DualFocus model against negative descriptions in textual queries. We augmented the textual queries by introducing two negative descriptions, derived from the predefined attribute table (Yang et al. 2023), to assess the models' ability to effectively exclude irrelevant information.

The empirical results, outlined in Table 5, show that DualFocus consistently outperforms competing methods in both Rank-1 accuracy and mean Average Precision (mAP) across all datasets. Specifically, DualFocus achieved Rank-1 accuracies of 80.05%, 70.42%, and 69.84% on each respective dataset. These results highlight the model's ability to maintain high precision and accuracy by effectively managing misleading descriptions. DualFocus's performance is enabled by its innovative architecture that combines Dynamic Tokenwise Similarity (DTS) and Dual Attribute Prompt Learning (DAPL), enhancing its handling of complex visual-textual interactions. This makes DualFocus highly effective in scenarios with imprecise or incorrect textual queries, maintaining high accuracy despite potential distractions.

Table 4: Ablation experimental results (%) on the effectiveness of each component in DualFocus. The "Baseline" represents the IRRA (Jiang and Ye 2023) model.

No.	Methods	Components			CUHK-PEDES			ICFG-PEDES			RSTPReid		
		\mathcal{L}_{dts}	\mathcal{DAPL}	\mathcal{L}_{diac}	Rank-1	Rank-5	Rank-10	Rank-1	Rank-5	Rank-10	Rank-1	Rank-5	Rank-10
1	Baseline				73.38	89.93	93.71	63.46	80.25	85.82	60.20	81.30	88.20
2	$+\mathcal{L}_{dts}$	✓			74.09	90.85	93.89	65.24	80.63	86.01	65.73	75.32	87.28
3	$+\mathcal{L}_{diac}$		✓		73.77	89.72	92.98	62.56	79.35	84.71	59.24	82.26	87.55
4	$+\mathcal{L}_{siam}$			✓	74.13	88.81	93.31	64.92	81.04	85.18	68.27	82.90	86.59
5	$+\mathcal{L}_{dts} + \mathcal{L}_{siam}$	✓		✓	74.65	88.37	93.62	64.49	81.38	85.04	68.62	81.75	87.30
6	$+\mathcal{DAPL}$		✓	✓	75.20	89.32	93.81	66.76	81.31	85.68	67.07	83.11	86.98
7	DualFocus	✓	✓	✓	77.43	90.73	94.20	67.87	82.06	87.33	69.12	86.68	92.31

Table 5: Performance (%) comparisons of SOTA (State-of-the-Art) Methods with Negative descriptions on the CUHK-PEDES, ICFG-PEDES, and RSTPReid Datasets.

Methods	CUHK-PEDES				ICFG-PEDES				RSTPReid			
	Rank-1	Rank-5	Rank-10	mAP	Rank-1	Rank-5	Rank-10	mAP	Rank-1	Rank-5	Rank-10	mAP
IRRA (Jiang and Ye 2023)	76.82	82.63	93.88	67.89	67.04	84.28	87.66	38.83	65.88	82.29	93.88	50.28
DECL (Li et al. 2023b)	77.06	84.27	94.16	68.43	68.73	84.42	88.58	39.42	64.16	84.45	92.01	53.81
RaSa (Bai et al. 2023)	78.64	85.42	94.67	69.28	69.27	84.35	89.44	40.21	67.17	85.45	91.19	54.97
APTM (Yang et al. 2023)	79.53	88.29	94.91	69.34	70.18	84.42	91.22	40.96	69.07	84.47	95.32	55.20
DualFocus(Ours)	80.05	87.65	96.48	70.02	70.42	84.68	89.59	41.37	69.84	87.96	94.62	56.98

Table 6: Performance Comparison on PA-100K.

Method	mA	Acc	Prec	Rec	F1
HP-net (Liu et al. 2017)	74.21	72.19	82.97	82.09	82.53
strongBaseline (Jia et al. 2020)	79.38	78.56	89.41	84.78	86.55
ALM (Tang et al. 2019)	80.68	77.08	84.21	88.84	86.46
RethinkPAR (Jia et al. 2021)	81.61	79.45	87.66	87.59	87.62
APTM (Yang et al. 2023)	82.58	80.17	88.31	87.84	88.07
DualFocus (Ours)	83.24	79.66	89.72	85.23	87.94

Pedestrian Attribute Recognition

Pedestrian attribute recognition focuses on identifying the attributes of target individuals from pedestrian images. We utilize the attribute prompt learning component of DualFocus to predict the attributes of images from the PA-100K dataset. Following a similar approach to APTM (Yang et al. 2023), we calculate the matching probability between each image and its corresponding attribute prompts for ranking. A higher matching probability indicates that the image is more likely to contain the associated attribute. Our method achieves competitive results, as demonstrated in Table 6.

The results validate the effectiveness of our DualFocus framework. DualFocus achieves a 0.66% improvement in mA compared to APTM (Yang et al. 2023) and a 0.31% improvement in precision compared to the strongBaseline (Jia et al. 2020). A recent study, PATH (Chen et al. 2023), reports an mA of 90.80%. However, since PATH (Tang et al. 2023) utilizes a more powerful backbone and additional data, we exclude it from our comparison to ensure fairness.

Comparisons on the domain generalization task

We conducted a rigorous evaluation of our DualFocus framework on the CUHK-PEDES and ICFG-PEDES datasets to assess its domain generalization capabilities. The

Table 7: Cross-Domain performance (%) between CUHK-PEDES and ICFG-PEDES. Here "C" denotes CUHK-PEDES, while "T" represents ICFG-PEDES.

Method	C → I			I → C		
	R@1	R@5	R@10	R@1	R@5	R@10
SSAN (Ding et al. 2021)	29.24	49.00	58.53	21.07	38.94	48.54
IRRA (Jiang and Ye 2023)	41.67	61.06	69.24	30.36	52.86	65.51
DCEL (Li et al. 2023b)	43.31	62.29	70.31	32.35	54.86	65.51
DualFocus(Ours)	50.47	68.62	74.60	45.34	62.67	75.43

results, detailed in Table 7, show that DualFocus substantially outperforms contemporary models like SSAN (Ding et al. 2021), IRRA (Jiang and Ye 2023), and DCEL (Li et al. 2023b). For instance, DualFocus achieved a Rank-1 accuracy of 50.47% when trained on CUHK-PEDES and tested on ICFG-PEDES, notably higher than its competitors. This performance highlights DualFocus's strength in handling domain variations and its ability to generalize well across different data distributions, owing to its innovative architecture that effectively integrates visual and textual data, enhancing adaptability and robustness in real-world scenarios.

Conclusion and Limitations

In this paper, we introduce DualFocus, a framework designed to enhance TPR by integrating plausible descriptions. By leveraging DAPL and DTS loss, DualFocus achieves precise attribute alignment and fine-grained matching, leading to a significant performance boost for TPR systems.

However, the current reliance on a predefined list of attributes to create negative examples during training limits the model's ability to capture the full diversity and complexity of natural language descriptions and real-world scenarios.

ios. This limitation impacts the model’s versatility and practical applicability, emphasizing the need for more sophisticated methods to generate negative descriptions that better reflect the nuances of real-world data. In summary, while DualFocus represents a significant step forward in TPR by effectively integrating linguistic and visual data, further advancements are necessary to fully realize its potential in more diverse and complex environments.

References

Bai, Y.; Cao, M.; Gao, D.; Cao, Z.; Chen, C.; Fan, Z.; Nie, L.; and Zhang, M. 2023. RaSa: relation and sensitivity aware representation learning for text-based person search. In *Proceedings of the Thirty-Second International Joint Conference on Artificial Intelligence*, 555–563.

Caron, M.; Touvron, H.; Misra, I.; Jégou, H.; Mairal, J.; Bojanowski, P.; and Joulin, A. 2021. Emerging properties in self-supervised vision transformers. In *Proceedings of the IEEE/CVF international conference on computer vision*, 9650–9660.

Chen, D.; Li, H.; Liu, X.; Shen, Y.; Shao, J.; Yuan, Z.; and Wang, X. 2018. Improving deep visual representation for person re-identification by global and local image-language association. In *ECCV*, 54–70.

Chen, W.; Xu, X.; Jia, J.; Luo, H.; Wang, Y.; Wang, F.; Jin, R.; and Sun, X. 2023. Beyond Appearance: a Semantic Controllable Self-Supervised Learning Framework for Human-Centric Visual Tasks. In *CVPR*, 15050–15061.

Chen, X.; Fan, H.; Girshick, R.; and He, K. 2020. Improved baselines with momentum contrastive learning. *arXiv preprint arXiv:2003.04297*.

Chen, Y.; Zhang, G.; Lu, Y.; Wang, Z.; and Zheng, Y. 2022. TIPCB: A simple but effective part-based convolutional baseline for text-based person search. *Neurocomputing*, 494: 171–181.

Dai, W.; Li, J.; Li, D.; Tiong, A. M. H.; Zhao, J.; Wang, W.; Li, B.; Fung, P.; and Hoi, S. 2023. InstructBLIP: Towards General-purpose Vision-Language Models with Instruction Tuning. *arXiv:2305.06500*.

Ding, Z.; Ding, C.; Shao, Z.; and Tao, D. 2021. Semantically self-aligned network for text-to-image part-aware person re-identification. *arXiv preprint arXiv:2107.12666*.

Farooq, A.; Awais, M.; Kittler, J.; and Khalid, S. S. 2022. AXM-Net: Implicit Cross-Modal Feature Alignment for Person Re-identification. In *AAAI*, volume 36, 4477–4485.

Fujii, T.; and Tarashima, S. 2023. BiLMA: Bidirectional Local-Matching for Text-based Person Re-identification. In *Proceedings of the IEEE/CVF International Conference on Computer Vision*, 2786–2790.

Han, X.; He, S.; Zhang, L.; and Xiang, T. 2021. Text-based person search with limited data. *arXiv preprint arXiv:2110.10807*.

He, K.; Fan, H.; Wu, Y.; Xie, S.; and Girshick, R. 2020. Momentum contrast for unsupervised visual representation learning. In *Proceedings of the IEEE/CVF conference on computer vision and pattern recognition*, 9729–9738.

Imambi, S.; Prakash, K. B.; and Kanagachidambaresan, G. 2021. PyTorch. *Programming with TensorFlow: Solution for Edge Computing Applications*, 87–104.

Jia, J.; Huang, H.; Chen, X.; and Huang, K. 2021. Rethinking of pedestrian attribute recognition: A reliable evaluation under zero-shot pedestrian identity setting. *arXiv preprint arXiv:2107.03576*.

Jia, J.; Huang, H.; Yang, W.; Chen, X.; and Huang, K. 2020. Rethinking of pedestrian attribute recognition: Realistic datasets with efficient method. *arXiv preprint arXiv:2005.11909*.

Jiang, D.; and Ye, M. 2023. Cross-Modal Implicit Relation Reasoning and Aligning for Text-to-Image Person Retrieval. In *Proceedings of the IEEE/CVF Conference on Computer Vision and Pattern Recognition*, 2787–2797.

Kingma, D. P.; and Ba, J. 2015. Adam: A Method for Stochastic Optimization. In *ICLR (Poster)*.

Li, J.; Li, D.; Savarese, S.; and Hoi, S. 2023a. Blip-2: Bootstrapping language-image pre-training with frozen image encoders and large language models. *arXiv preprint arXiv:2301.12597*.

Li, J.; Selvaraju, R.; Gotmare, A.; Joty, S.; Xiong, C.; and Hoi, S. C. H. 2021. Align before fuse: Vision and language representation learning with momentum distillation. *Advances in neural information processing systems*, 34: 9694–9705.

Li, S.; Xiao, T.; Li, H.; Zhou, B.; Yue, D.; and Wang, X. 2017. Person search with natural language description. In *CVPR*, 1970–1979.

Li, S.; Xu, X.; Yang, Y.; Shen, F.; Mo, Y.; Li, Y.; and Shen, H. T. 2023b. DCEL: Deep Cross-modal Evidential Learning for Text-Based Person Retrieval. In *Proceedings of the 31st ACM International Conference on Multimedia*, 6292–6300.

Liu, X.; Zhao, H.; Tian, M.; Sheng, L.; Shao, J.; Yi, S.; Yan, J.; and Wang, X. 2017. Hydraplus-net: Attentive deep features for pedestrian analysis. In *ICCV*, 350–359.

Ma, Y.; Sun, X.; Ji, J.; Jiang, G.; Zhuang, W.; and Ji, R. 2023. Beat: Bi-directional One-to-Many Embedding Alignment for Text-based Person Retrieval. In *Proceedings of the 31st ACM International Conference on Multimedia*, 4157–4168.

Radford, A.; Kim, J. W.; Hallacy, C.; Ramesh, A.; Goh, G.; Agarwal, S.; Sastry, G.; Askell, A.; Mishkin, P.; Clark, J.; et al. 2021. Learning transferable visual models from natural language supervision. In *International conference on machine learning*, 8748–8763. PMLR.

Sennrich, R.; Haddow, B.; and Birch, A. 2015. Neural machine translation of rare words with subword units. *arXiv preprint arXiv:1508.07909*.

Shao, Z.; Zhang, X.; Fang, M.; Lin, Z.; Wang, J.; and Ding, C. 2022. Learning granularity-unified representations for text-to-image person re-identification. In *Proceedings of the 30th ACM International Conference on Multimedia*, 5566–5574.

Shu, X.; Wen, W.; Wu, H.; Chen, K.; Song, Y.; Qiao, R.; Ren, B.; and Wang, X. 2022. See finer, see more: Implicit

modality alignment for text-based person retrieval. In *European Conference on Computer Vision*, 624–641. Springer.

Tang, C.; Sheng, L.; Zhang, Z.; and Hu, X. 2019. Improving pedestrian attribute recognition with weakly-supervised multi-scale attribute-specific localization. In *ICCV*, 4997–5006.

Tang, S.; Chen, C.; Xie, Q.; Chen, M.; Wang, Y.; Ci, Y.; Bai, L.; Zhu, F.; Yang, H.; Yi, L.; et al. 2023. Humanbench: Towards general human-centric perception with projector assisted pretraining. In *Proceedings of the IEEE/CVF Conference on Computer Vision and Pattern Recognition*, 21970–21982.

Wang, Z.; Fang, Z.; Wang, J.; and Yang, Y. 2020. Vitaa: Visual-textual attributes alignment in person search by natural language. In *ECCV*, 402–420.

Wang, Z.; Zhu, A.; Xue, J.; Wan, X.; Liu, C.; Wang, T.; and Li, Y. 2022a. Caibc: Capturing all-round information beyond color for text-based person retrieval. In *Proceedings of the 30th ACM International Conference on Multimedia*, 5314–5322.

Wang, Z.; Zhu, A.; Xue, J.; Wan, X.; Liu, C.; Wang, T.; and Li, Y. 2022b. Look before you leap: Improving text-based person retrieval by learning a consistent cross-modal common manifold. In *Proceedings of the 30th ACM International Conference on Multimedia*, 1984–1992.

Yan, S.; Dong, N.; Zhang, L.; and Tang, J. 2022. Clip-driven fine-grained text-image person re-identification. *arXiv preprint arXiv:2210.10276*.

Yang, S.; Zhou, Y.; Wang, Y.; Wu, Y.; Zhu, L.; and Zheng, Z. 2023. Towards Unified Text-based Person Retrieval: A Large-scale Multi-Attribute and Language Search Benchmark. In *Proceedings of the 2023 ACM on Multimedia Conference*.

Yao, L.; Huang, R.; Hou, L.; Lu, G.; Niu, M.; Xu, H.; Liang, X.; Li, Z.; Jiang, X.; and Xu, C. 2021. Filip: Fine-grained interactive language-image pre-training. *arXiv preprint arXiv:2111.07783*.

Ye, M.; Shen, J.; Lin, G.; Xiang, T.; Shao, L.; and Hoi, S. C. 2021. Deep learning for person re-identification: A survey and outlook. *IEEE Transactions on Pattern Analysis and Machine Intelligence (TPAMI)*.

Yu, J.; Wang, Z.; Vasudevan, V.; Yeung, L.; Seyedhosseini, M.; and Wu, Y. 2022. Coca: Contrastive captioners are image-text foundation models. *arXiv preprint arXiv:2205.01917*.

Zheng, Z.; Zheng, L.; Garrett, M.; Yang, Y.; Xu, M.; and Shen, Y.-D. 2020. Dual-path convolutional image-text embeddings with instance loss. *ACM Transactions on Multimedia Computing, Communications, and Applications (TOMM)*, 16(2): 1–23.

Zhu, A.; Wang, Z.; Li, Y.; Wan, X.; Jin, J.; Wang, T.; Hu, F.; and Hua, G. 2021. Dssl: Deep surroundings-person separation learning for text-based person retrieval. In *Proceedings of the 29th ACM International Conference on Multimedia*, 209–217.